



Research and Innovation action

March, 2024

## **D1.2 - Technical specifications requested to the PTES section based on a preliminary design**

### **Preliminary Design and Scenarios**

Version n°1

Authors:

Mario Petrollese, Mostafa Esmaeili Shayan (UNICA, Italy)



This project has received funding from the European Union's Horizon 2020 Research and Innovation Program under Grant Agreement 963530.

The content of this document reflects only the author's view. The European Commission is not responsible for any use that may be made of the information it contains.

# Executive Summary

This study investigates the potential of pumped thermal energy storage (PTES) systems to address the energy and agricultural requirements of African communities while simultaneously promoting sustainable development and the integration of renewable energy sources. We employ different designs of PTES systems to optimize efficiency, scalability, and compatibility with renewable energy sources. To respond to demand, these systems use excess thermal energy. Advanced control strategies enhance energy management efficiency in both on-grid and off-grid systems. PTES technicalities encompass storage capacity, temperature range, heat transfer fluid, and system components. The choice of heat transfer fluid has a direct impact on the system's efficiency and the environment. As the performance and reliability of materials and technologies improve, PTES systems become more feasible for widespread adoption. The study analyzes the technical specifications of the PTES storage section in a step-by-step manner. The preliminary PTES system was designed using MATLAB and GAMS, taking into account the energy and agricultural requirements of African communities and their compatibility with renewable energy sources. The PTES system utilizes both renewable and non-renewable energy sources. Power blocks can function as either heat pumps or heat engines, while thermal energy storage (TES) reservoirs are designed to store energy at both low and high temperatures. During the charging process, electrical energy is used to transfer heat from the low-temperature reservoir to the high-temperature reservoir. Discharging is the process of converting thermal energy into electricity. The study also examines the applications of PTES systems, such as desalination, cold storage, and the production of green ammonia. The size of subsystems is determined by analyzing case studies and considering user requests. Mathematical models assess the performance of plants under specific operational conditions. The primary conclusions indicate that the heat pump should possess a nominal power that is at least 50% greater than that of the heat engine. Enhancing the  $P_r$  to 2.5 times significantly improve the efficiency of the system. The study presents a model that optimizes the amount of curtailed energy and accurately matches the observed data. The proposed RES-PTES configuration comprises a 250 kW photovoltaic system, a 70 kW heat pump, a 26 kW heat engine, and a 26 kW/26 kWh battery energy storage system (BESS). It is anticipated that this configuration will fulfill 80-90% of the energy demand. An examination of authorized load curtailment reveals that as the curtailment increases, the quantity of energy that is curtailed decreases. The ideal size for a heat pump is typically 1.25 to 2.75 times the power of the heat engine. This relationship can be accurately represented by an exponential equation that describes how the initial cost of the system is affected by the amount of load curtailment allowed. The suggested system, utilizing the preliminary design and farm survey data, consists of a photovoltaic (PV) system that spans an area of 1250-1350 m<sup>2</sup> (equivalent to 0.7-0.8 hectares) and has an annual energy generation capacity of 300-350 MWh. Around 30-35% of the produced energy will be reduced to match the present demand, and the BESS should have the capacity to store sufficient energy to fulfill one hour of the highest power usage, taking into account a potential rise in power demand ranging from 25% to 75%.

**Keywords:** Pumped Thermal Energy Storage (PTES), Hybrid Renewable Energy, PTES-RES, Thermal Energy Storage (TES), Concentrated Solar Power (CSP).

## LITERATURE REVIEW

Pumped thermal energy storage (PTES) systems have emerged as a promising solution to address the energy and agricultural needs of African communities while promoting sustainable development and renewable energy integration. This comprehensive review delves into the design, operation, and technical specifications of PTES systems, highlighting their potential to revolutionize the energy landscape in African communities.

### 1. Design of PTES Systems

The design of PTES systems encompasses various configurations, with novel integrated designs being proposed for optimal utilization of excess thermal energy. Crucial design considerations include system efficiency, scalability, and compatibility with renewable energy sources such as solar and wind power [1]. By carefully addressing these factors, PTES systems can be tailored to meet the unique energy demands of African communities.

### 2. Operation of PTES Systems

PTES systems operate on the principle that excess thermal energy is used to store and release energy as needed, effectively balancing supply and demand. Advanced control strategies play a significant role in ensuring efficient operation and energy management, maximizing the benefits of these systems for both on-grid [2] and off-grid [3] applications in African communities.

### 3. Technical Specifications

The technical aspects of PTES systems involve essential components such as storage capacity, temperature range, heat transfer fluid, and system components. Storage capacity and temperature range are critical determinants of system performance, while the choice of heat transfer fluid can significantly impact system efficiency and environmental footprint [4]. Additionally, advances in materials and technologies contribute to enhancing the performance and reliability of PTES systems, making them increasingly viable for widespread adoption.

### 4. State-of-the-Art in PTES Technology

Research papers and case studies provide valuable insights into the latest advancements, challenges, and potential applications of PTES technology [5]. Ongoing research efforts aim to address existing challenges and further improve the performance of PTES systems, paving the way for their successful implementation in African communities. By leveraging these advancements, PTES systems can play a pivotal role in driving sustainable development and renewable energy integration across the continent.

## MATERIALS AND METHODS

To provide a comprehensive analysis of the role of PTES systems in addressing the energy and agricultural needs of African communities sustainably, this study employs a multi-stage research approach. In this section, we focus on the technical specifications requested for the PTES storage section based on a preliminary design using the specialized software MATLAB and GAMS. The following subsections outline the materials and methods used for this specific task.

### 1. Preliminary Design and System Parameters

Based on the literature review and data collection, a preliminary design of the PTES system was developed, taking into account the energy and agricultural needs of African communities, as well as compatibility with renewable energy sources. The factors considered in CASE STUDY 1 (Nigerian small-scale farm), CASE STUDY 2 (Moroccan small-scale farm), and CASE STUDY 3 (Nigerian large-scale farm) encompassed meteorological data, energy consumption levels, and land sizes. Finally, a CASE STUDY 4 will be considered to investigate the potentiality of integrating PTES system with large ammonia power plant located in South of Morocco. The overview of the RES-PTES system is depicted in Figure 1. The system encompasses both renewable energy sources, such as solar-photovoltaic energy and wind energy, as well as non-renewable energy sources, such as diesel generators or electricity grid connections. The sources of power generation can encompass either AC or DC systems. In cases where the consumers and power producing sources differ, the function of the inverter becomes evident. Battery energy storage systems are designed to store renewable energy generated by renewable sources for consumption that is not connected to the main power grid.

The block diagram of the system Figure 1 depicts the incorporation of renewable power facilities with pumped thermal energy storage to fulfill the sustainable energy and agricultural needs of African communities. The PTES systems comprise a versatile power block that can operate as both a heat pump and a heat engine. These systems work in tandem with a TES system, which includes reservoirs at low temperatures (referred to as the cold tank, CT) and high temperatures (referred to as the hot tank, HT). During the charging process, electrical energy is used to transfer heat from a low temperature reservoir to a high temperature reservoir through a reverse power cycle. The CSP technology utilizes solar energy to directly supply heat to the hot tank. The system can effectively harness both the thermal and photovoltaic properties of solar radiation. On the other hand, during the discharging phase, the stored thermal energy is converted back into electrical energy using a power cycle. Simulation tools have been developed using MATLAB to design components and offer a comprehensive analysis of their performance in non-standard conditions. These tools are specifically designed for PTES, renewable power generating sources, RES generators, batteries, and other external heat sources. The integration of these simulated instruments into a comprehensive system model was undertaken in order to assess their efficacy in precisely monitoring heat and electricity grid profiles. This study involves a comprehensive examination of the design and performance simulation of the PTES section, along with the development of models for potential commodities that can be integrated into the PTES system. Based on the proposal, analyzed cases, and anticipated needs, three prospective foreign plants are being evaluated for independent or integrated integration with the system: a desalination plant,

which employs power and heat to generate desalinated water, thereby addressing the increasing demand for fresh water; a cold storage facility, which improves food security and sustainability by mitigating food losses caused by insufficient storage conditions; and a green ammonia manufacturing facility, which plays a vital role in fertilizer production within the agricultural and horticultural sectors, leveraging advancements in water electrolysis technologies that harness renewable electricity for the production of green hydrogen.

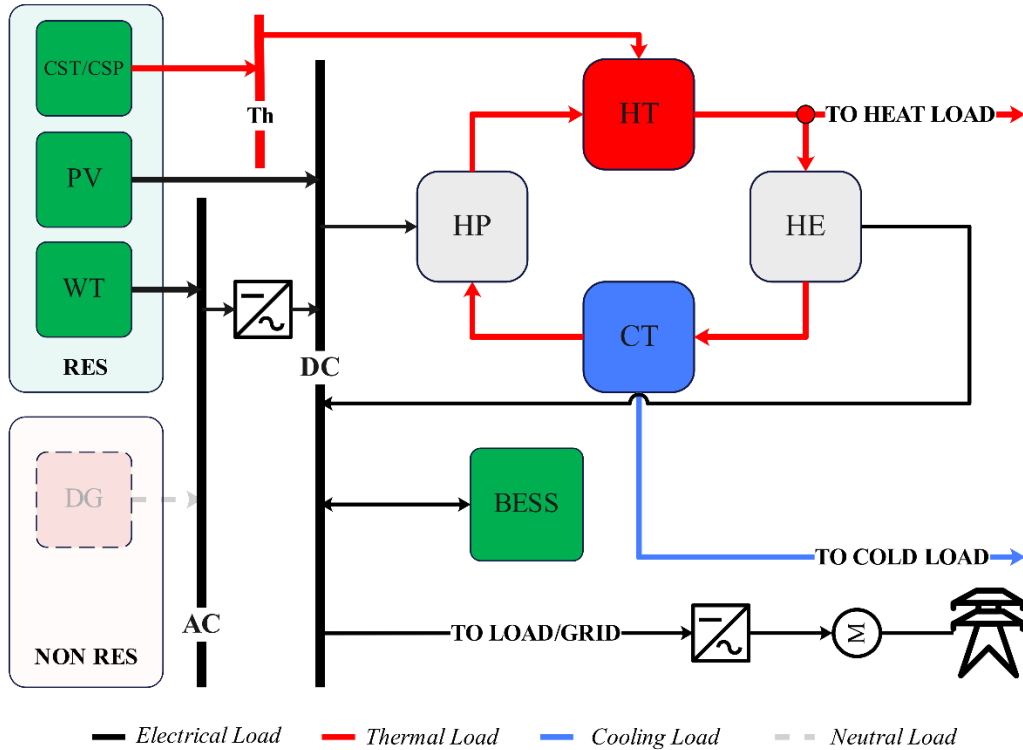


**Figure 1.** RES-PTES system's block diagram.

The dimensions of these three subsystems are defined by analyzing case studies and seeking input from possible users. Mathematical models are then created to evaluate the plant's performance during operation.

## 2. System Modeling

The provided Equation (1-1) is relevant to a Photovoltaic (PV) sub-array system, whereby the primary design parameter to be optimized is the quantity of sub-arrays, represented as  $n_s$ . The specified power output of each PV sub-array is 10 kilowatts (kW). In Matlab, the initial equation computes the power output of a photovoltaic sub-array at a specific time ( $t$ ). The outcome is contingent upon several factors, including the nominal power of the sub-array  $P_{PV,S,nom}$ , the Global Irradiance (GI) at time  $t$ , the Global Irradiance under Standard Test Conditions ( $GI_{STC}$ ), the temperature coefficient of power ( $\alpha_p$ ), that will be a negative number, the cell temperature at time  $t$  ( $T_{cell}(t)$ ), and the cell temperature under Standard Test Conditions ( $T_{cell,STC}$ ). The equation (1-2), as mathematically expressed in GAMS, computes the aggregate power generation of the

photovoltaic (PV) system ( $P_{PV}(t)$ ) at a specific time ( $t$ ). The calculation involves multiplying the power output of a single PV sub-array ( $P_{PV,s}(t)$ ), the efficiency of the inverter ( $\eta_{inv}(t)$ ), the derating factor of PV ( $f_{der,PV}$ ), and the number of sub-arrays ( $n_s$ ). The equation (1-3), which is also employed in GAMS, decomposes the overall power output of the PV system ( $P_{PV}(t)$ ) into four constituent elements: the power supplied to the load ( $P_{PV_D}(t)$ ), the power consumed by the heat pump ( $P_{PV_{HP}}(t)$ ), the power utilized for battery charging ( $P_{PV_{BC}}(t)$ ), and the power dissipated within the system ( $P_{PV_{lost}}(t)$ ). The utilization of PV power is limited due to its underutilization and inability to be stored, as the storage systems are fully charged.

$$P_{PV,s}(t) = P_{PV,s,nom} \cdot \frac{GI(t)}{GI_{STC}} \cdot [1 + \alpha_P \cdot (T_{cell}(t) - T_{cell,STC})] \quad \text{(Matlab)} \quad (1-1)$$

$$P_{PV}(t) = [P_{PV,s}(t) \cdot \eta_{inv}(t) \cdot f_{der,PV}] \cdot n_s \quad \text{(GAMS)} \quad (1-2)$$

$$P_{PV}(t) = P_{PV_D}(t) + P_{PV_{HP}}(t) + P_{PV_{BC}}(t) + P_{PV_{lost}}(t) \quad \text{(GAMS)} \quad (1-3)$$

The design parameter to be optimized in equation (1-4) is the quantity of wind turbines ( $n_{WT}$ ), with each wind turbine having a nominal power of 100 kW. The equation denotes the relationship between the power output of the wind turbine ( $P_{WT}(t)$ ) and the wind speed at the hub ( $ws_{hub}$ ). The power output is determined by applying a cubic equation to wind speeds ranging from 3 m/s to 12 m/s. A distinct cubic equation is employed for wind velocities ranging from 12 m/s to 25 m/s. The power output is zero for wind speeds below 3 m/s or above 25 m/s. The equation is executed via the MATLAB Version 23.2. (R2023b) Update 6.

The power output of the wind farm  $P_{WF}(t)$  is determined by multiplying the power output of the wind turbine ( $P_{WT}(t)$ ) by the ratio of the hub density ( $\rho_{hub}(t)$ ) to the reference density ( $\rho_{ref}$ ), and then multiplying it by the auxiliary loss factor ( $k_{aux}$ ) and the wake factor ( $k_W$ ). Finally, the resulting equation is multiplied by the number of wind turbines ( $n_{WT}$ ). The equation is executed via the GAMS software. The net power output of the wind farm ( $P_{WF}(t)$ ) is determined by aggregating the power outputs of various components, namely the direct demand power output ( $P_{WF_D}(t)$ ), the heat pump power output ( $P_{WF_{HP}}(t)$ ), the battery energy storage system (BESS) power output ( $P_{WF_{BC}}(t)$ ), the power that is neither usable nor stored is regarded as lost ( $P_{WF_{lost}}(t)$ ).

$$\begin{aligned} P_{WT}(t) &= 0.015 \cdot ws_{hub}^3(t) - 0.975 \cdot ws_{hub}^2(t) + 17.81 \cdot ws_{hub}(t) - 5.328 & 12 \frac{m}{s} \leq ws_{hub} \leq 25 \frac{m}{s} \\ P_{WT}(t) &= -0.3 \cdot ws_{hub}^3(t) + 6.63 \cdot ws_{hub}^2(t) - 33.23 \cdot ws_{hub}(t) + 50.94 & 3 \frac{m}{s} \leq ws_{hub} < 12 \frac{m}{s} \\ P_{WT}(t) &= 0 & ws_{hub} < 3 \frac{m}{s} \text{ or } ws_{hub} > 25 \frac{m}{s} \end{aligned} \quad (1-4)$$

$$P_{WF}(t) = \left[ P_{WT}(t) \cdot \frac{\rho_{hub}(t)}{\rho_{ref}} \cdot (1 - k_{aux}) \cdot (1 - k_W) \right] \cdot n_{WT} \quad (1-5)$$

$$P_{WF}(t) = P_{WF_D}(t) + P_{WF_{HP}}(t) + P_{WF_{BC}}(t) + P_{WF_{lost}}(t) \quad (1-6)$$

Equation (1-7) describes a Concentrated Solar Thermal (CST) plant, characterized by a central tower encircled by a polar heliostat field and equipped with a cavity receiver. The optimization of

the design parameter for the heliostat field is focused on the overall mirror area ( $A_{HF}$ ), with each individual heliostat area of  $120 \text{ m}^2$ . The heat loss ( $\dot{Q}_{lost}(t)$ ) from the receiver is determined by the equation (1-7), which takes into account several parameters including the receiver area ( $A_{rec}$ ), the receiver emissivity ( $\epsilon_{rec}$ ), the Stefan-Boltzmann constant ( $\sigma_{SB}$ ), the receiver temperature ( $T_{rec}$ ), the ambient temperature ( $T_{amb}$ ), the overall heat transfer coefficient ( $U_L$ ), and the time-dependent ambient temperature ( $T_{amb}(t)$ ). The equation (1-7) is executed via the Matlab software. The equation (1-8) represents the heat rate output ( $\dot{Q}_{CST}(t)$ ) of the CST plant. It is determined by multiplying the solar optical efficiency ( $\eta_{opt}(t)$ ), the direct normal irradiance (DNI), and the total mirror area of the heliostat field ( $A_{HF}$ ), and subtracting the heat losses ( $\dot{Q}_{lost}(t)$ ) and defocusing losses ( $\dot{Q}_{def}(t)$ ). In instances where the solar field's potential thermal power cannot be immediately utilized or stored, purposeful defocusing of mirrors is employed. The equation (1-8) is executed via the GAMS software. Furthermore, there are limitations imposed on the heat output of the CST plant. The desired heat output should fall within the defined range, which is calculated by multiplying the minimum CST heat output ( $\dot{Q}_{CST_{min}}$ ) by the On/Off status of the CST. The binary variable  $Y_{CST}(t)$  is assigned a value of 1 throughout the operation of CST and the maximum CST heat output ( $\dot{Q}_{CST_{nom}}$ ) by the On/Off status. GAMS is also utilized to implement these limitations.

$$\dot{Q}_{lost}(t) = A_{rec} \cdot \left[ \epsilon_{rec} \cdot \sigma_{SB} \cdot \left( T_{rec}^4 - T_{amb}^4(t) \right) + U_L \cdot \left( T_{rec} - T_{amb}(t) \right) \right] \text{ (Matlab)} \quad (1-7)$$

$$\dot{Q}_{CST}(t) = \eta_{opt}(t) \cdot DNI(t) \cdot A_{HF} - \dot{Q}_{def}(t) - \dot{Q}_{lost}(t) \text{ (GAMS)} \quad (1-8)$$

$$\dot{Q}_{CST_{min}} \cdot Y_{CST}(t) \leq \dot{Q}_{CST}(t) \leq \dot{Q}_{CST_{nom}} \cdot Y_{CST}(t) \text{ (GAMS)} \quad (1-9)$$

The provided equation pertains to a PTES system, wherein there exist multiple design parameters that necessitate optimization. These parameters encompass the storage capacity, heat pump rated power, and heat engine rated power. The power input of the heat pump ( $P_{HP}(t)$ ) at a specific time ( $t$ ) is denoted by the equation (1-10) and  $P_{HP}(t)$ , which is derived by adding the power output from the PV system ( $P_{PV_{HP}}(t)$ ), the power output from the wind turbine ( $P_{WT_{HP}}(t)$ ), and the further power that should be requested but the RES generators cannot satisfy  $P_{HP_{curtailed}}(t)$ . The equation is executed via the GAMS software. Constraints are established for the power output ( $P_{HP}(t)$ ) of the heat pump.

The power output should fall within the range defined by the product of the minimum heat pump power ( $P_{HP_{min}}$ ) and the heat pump On/Off state ( $Y_{HP}(t)$ ), as well as the maximum heat pump power ( $P_{HP_{nom}}$ ) and the heat pump On/Off state. This constraint, implemented with the GAMS software by equation (1-11), should be nonlinear if the heat pump rated power ( $P_{HP_{nom}}$ ) is considered as a variable to be optimized. To maintain the formulation as MILP, it was decided to convert the  $P_{HP_{nom}}$  into a parameter and carry out optimizations for different values of such parameter. The heat output of the heat pump ( $\dot{Q}_{HP}(t)$ ) at a specific time ( $t$ ), represented by equation (1-12), is determined from the heat pump power input ( $P_{HP}(t)$ ) by means of the coefficient of performance

(COP). Actually, this equation would exhibit non-linearity since the COP varies when the heat pump operates at part-load conditions but, in this preliminary analysis it is considered constant.

The power output of the heat engine ( $P_{HE}(t)$ ) at a specific moment ( $t$ ), denoted by the equation (1-13), is determined by adding the power output from the heat engine directly to satisfy a share of the load demand ( $P_{HE,D}(t)$ ) and the power output used to charge the battery bank ( $P_{HE,BC}(t)$ ). Like the heat pump, the heat engine is subject to limitations on its power output ( $P_{HE}(t)$ ). The power output should fall within the range defined by the product of the minimum heat engine power output ( $P_{HE_{min}}$ ) and the heat engine On/Off status ( $Y_{HE}$ ), as well as the maximum heat engine power output ( $P_{HE_{nom}}$ ) and the heat engine On/Off status ( $Y_{HE}$ ). Like the heat pump, the constraint should be nonlinear. However, to avoid the introduction of nonlinearity, it is assumed that the heat engine rated power is equal to the maximum load demand. In equation (1-15),  $\dot{Q}_{HE}(t)$  denotes the heat requested by the heat engine ( $\dot{Q}_{HE}$ ) at a specific time ( $t$ ) and is determined by means of the definition of a heat engine efficiency ( $\eta_{HE}$ ), which is considered constant in this phase. An additional constraint is implemented in GAMS by equation (1-16), which establishes that the heat engine and the heat pump cannot operate simultaneously.

The variables  $Q_{HT}(t)$  and  $Q_{CT}(t)$  denote the total heat stored in the hot tank and cold tank at a specific time ( $t$ ), respectively. The variation over time of accumulated heat in the hot tank is determined by equation (1-17), which takes into account the heat inputs and outputs from different sources. These sources include the CST heat output ( $\dot{Q}_{CST}(t)$ ) and HP heat output ( $\dot{Q}_{HP}(t)$ ), while heat demand includes the HE heat output ( $\dot{Q}_{HE}(t)$ ), and the eventual heat request from the user ( $\dot{Q}_{HT,REQ}(t)$ ). The starting value of the accumulated heat in the hot tank ( $Q_{HT}(t = 1)$ ) is subject to limitations that ensure it is less than or equal to the accumulated heat at the end of the year ( $Q_{HT}(t = 8760)$ ), as reported in equation (1-18). Moreover, as reported in equation (1-19), the stored heat cannot exceed the maximum capacity of the hot tank ( $Q_{HT,max}$ ). Similar constraints are imposed for the cold tank. Unlike the hot tank, the only source producing cold energy is the heat pump at the evaporator side (calculated based on the HP COP), while the only demand, in case of a Rankine based PTES system, comes from an eventual cold energy request by the user ( $\dot{Q}_{CT,REQ}(t)$ ).

$$P_{HP}(t) = P_{PV_{HP}}(t) + P_{WT_{HP}}(t) + P_{HP_{curtailed}}(t) \text{ (GAMS)} \quad (1-10)$$

$$P_{HP_{min}} \cdot Y_{HP}(t) \leq P_{HP}(t) \leq P_{HP_{nom}} \cdot Y_{HP}(t) \text{ (GAMS- non linear)} \quad (1-11)$$

$$\dot{Q}_{HP}(t) = COP \cdot P_{HP}(t) \text{ (GAMS – nonlinear)} \quad (1-12)$$

$$P_{HE}(t) = P_{HE,D}(t) + P_{HE,BC}(t) \text{ (GAMS)} \quad (1-13)$$

$$P_{HE_{min}} \cdot Y_{HE}(t) \leq P_{HE}(t) \leq P_{HE_{nom}} \cdot Y_{HE}(t) \text{ (GAMS – non linear)} \quad (1-14)$$

$$\dot{Q}_{HE}(t) = P_{HE}(t) / \eta_{HE} \text{ (GAMS – non linear)} \quad (1-15)$$

$$Y_{HE}(t) - Y_{HP}(t) \leq 1 \text{ (GAMS)} \quad (1-16)$$

$$Q_{HT}(t) = Q_{HT}(t - 1) + [\dot{Q}_{CST}(t) + \dot{Q}_{HP}(t) - \dot{Q}_{HE}(t) - \dot{Q}_{HT,REQ}(t)] \cdot \Delta t \text{ (GAMS)} \quad (1-17)$$

$$Q_{HT}(t = 1) \leq Q_{HT}(t = 8760) \text{ (GAMS)} \quad (1-18)$$

$$Q_{HT}(t) \leq Q_{HT,max} \text{ (GAMS)} \quad (1-19)$$

$$Q_{CT}(t) = Q_{CT}(t - 1) + [\dot{Q}_{HP}(t)(COP - 1)/COP - \dot{Q}_{CT,REQ}(t)] \cdot \Delta t \text{ (GAMS)} \quad (1-20)$$

$$Q_{CT}(t = 1) \leq Q_{CT}(t = 8760) \text{ (GAMS)} \quad (1-21)$$

$$Q_{CT}(t) \leq Q_{CT,max} \text{ (GAMS)} \quad (1-22)$$

The equation (1-23) is representative of the power balance and it denotes the aggregate power outputs derived from the photovoltaic system ( $P_{PV,D}(t)$ ) to demands, wind turbine ( $P_{WT,D}(t)$ ), heat engine ( $P_{HE,D}(t)$ ), and battery discharge to demands ( $P_{BD}(t)$ ). The sum can be calculated by subtracting the curtailed power demand ( $P_{L,curtailed}(t)$ ) from the power demand from the load ( $P_L(t)$ ). The equation is executed via the GAMS software. The equation (1-24) represents the energy stored in the battery ( $E_B(t)$ ) at a specific time ( $t$ ). It is determined by considering the energy stored in the battery at the previous time step ( $E_B(t - 1)$ ), the power inputs into the battery from the photovoltaic system ( $P_{PV,BC}(t)$ ), wind turbine ( $P_{WT,BC}(t)$ ), and heat engine ( $P_{HE,BC}(t)$ ), the battery charging efficiency ( $\eta_{BC}$ ), and the battery discharge power ( $P_{BD}(t)$ ) divided by the battery discharge efficiency ( $\eta_{BD}$ ). The equation is executed via the GAMS software. A limitation exists whereby the energy stored in the battery ( $E_B(t)$ ) at a specific time ( $t$ ) must be less than or equal to the maximum energy capacity of the battery ( $E_{B,max}$ ). This constraint serves to prevent the battery from beyond its maximum capacity in terms of stored energy. GAMS is utilized to implement this limitation.

$$P_{PV,D}(t) + P_{WT,D}(t) + P_{HE,D}(t) + P_{BD}(t) = P_L(t) - P_{L,curtailed}(t) \text{ (GAMS)} \quad (1-23)$$

$$E_B(t) = E_B(t - 1) + [P_{PV,BC}(t) + P_{WT,BC}(t) + P_{HE,BC}(t)] \cdot \eta_{BC} - P_{BD}(t) \cdot \eta_{BD} \text{ (GAMS)} \quad (1-24)$$

$$E_B(t) \leq E_{B,max} \text{ (GAMS)} \quad (1-25)$$

The given equations (1-26) and (1-27) denote constraints imposed on the load curtailments. Specifically, it is required that the daily load demand not satisfied ( $\sum P_{L,curt}(t)$ ) does not exceed a fraction ( $X_{curt}$ ) of the daily load demand ( $\sum P_L(t)$ ). A similar constraint is implemented for limiting the share of daily energy requested by the heat pump that is not satisfied.

$$\sum_{t=(day-1) \cdot 24+1}^{day \cdot 24} P_{L,curtailed}(t) \leq X_{curt} \cdot \sum_{t=(day-1) \cdot 24+1}^{day \cdot 24} P_L(t) \text{ (GAMS)} \quad (1-26)$$

$$\sum_{t=(day-1) \cdot 24+1}^{day \cdot 24} P_{HP,curtailed}(t) \leq X_{curt} \cdot \sum_{t=(day-1) \cdot 24+1}^{day \cdot 24} \dot{Q}_{CT,REQ}(t)/(COP - 1) \text{ (GAMS)} \quad (1-27)$$

Equation (1-28) presents the objective function, which seeks to minimize the overall cost by optimizing several design parameters. These factors include the quantity of photovoltaic (PV) modules, wind turbines, heliostat field area, thermal energy storage capabilities, and battery energy storage capacity. The objective function does not incorporate the rated powers of the heat pump (HP) and heat engine (HE) as they are not considered as variables within this particular formulation to keep a linear problem formulation:

$$\text{Min Cost} = c_{PV}n_s + c_{WT}n_{WT} + c_{HF}A_{HF} + c_{TES}(Q_{HT,max} + Q_{CT,max}) + c_B E_{B,max} \quad (1-28)$$

The variables  $n_s$  and  $n_{WT}$  reflect the number of PV panels and WTs, respectively, whereas  $A_{HF}$  denotes the size of the heliostat field. The  $Q_{HT,max}$  and  $Q_{CT,max}$  represent the maximum thermal energy storage capacity for the hot tank (HT) and cold tank (CT) storage, respectively. The battery's maximum energy capacity is represented by the symbol  $E_{B,max}$ . The unit expenses associated with each component are represented by the specific cost  $c_{PV}$ ,  $c_{WT}$ ,  $c_{HF}$ ,  $c_{TES}$ , and  $c_B$ .

### 3. Algorithm Architecture

An optimization tool is developed to determine the desired characteristics of the PTES storage section, such as storage capacity, charging and discharging rating power etc. based on the demands of the end-users. This tool will also determine the optimal capacity ratio of the RES plant by applying specific objective functions. The formulation of an optimization problem is to identify the optimal combination of variables by minimizing an objective function. The implementation of the model has been carried out using MATLAB, employing the GAMS optimization software. CPLEX solves the optimization problem as Mixed Integer Linear Programming (MILP). GAMS is a powerful tool for mathematical programming, enabling the formulation and solution of complex optimization problems. The variables and parameters are classified into different categories such as sets, parameters, positive variables, binary variables, integer variables, SOS2 variables, and variables. The definitions of each variable and parameter are provided to give a clear understanding of their role in the optimization problem.

During the optimization phase, various parameters have been modeled and optimized, including the necessary nominal power for the photovoltaic solar power plant and wind turbines, the capacity of battery energy storage, and other factors such as the size of the heat tank and cold tank, as well as rated power of the heat engine and the heat pump. The optimization of this model can be achieved by utilizing case study meteorological data and considering the access conditions to various sources of renewable energy. The code initially establishes the main characteristics of a PV subarray and of a wind turbine taken as reference. Subsequently, the electricity generation from these sources is simulated by utilizing weather data. The optimization of a battery energy storage system enables the model to effectively handle the intermittent nature of solar and wind energy sources. In the PTES system, the code additionally establishes the efficiencies for battery charging and discharging, as well as the nominal efficiency of the heat engine. The system variables categories presented in Table 1. Each category represents a crucial component of the energy system being studied.

As indicated in Table 1. The system's variables can be classified into five primary categories: Power Variables, Thermal Power Variables, Energy Storage Variables, On/Off Status Variables, and Design Variables. Power variables refer to the electrical power that is produced, consumed, or transmitted within a given system.

**Table 1.** The GAMS and MATLAB software utilize variables for the optimization of RES-PTES.

Category	Variables	Type
Power Variables	$P_{PVD}$	Positive, Time-Dependent
	$P_{PVHP}$	
	$P_{PVBC}$	
	$P_{PVlost}$	
	$P_{WFD}$	
	$P_{WFHP}$	
	$P_{WFBC}$	
	$P_{WFlost}$	
	$P_{HP}$	
	$P_{HE}$	
	$P_{HED}$	
	$P_{HEBC}$	
Thermal Power Variables	$P_{Lcurtailed}$	Positive, Time-Dependent
	$P_{HPcurtailed}$	
	$P_{BD}$	
	$\dot{Q}_{HP}$	
	$\dot{Q}_{HE}$	
Energy Storage Variables	$\dot{Q}_{CST}$	Positive, Time-Dependent
	$\dot{Q}_{def}$	
	$Q_{HT}$	
	$Q_{CT}$	
On/Off Status Variables	$E_B$	Binary, Time-Dependent
	$Y_{HP}$	
	$Y_{HE}$	
Design Variables	$Y_{CST}$	Positive, scalar
	$n_s$	
	$n_{WT}$	
	$A_{HF}$	
	$Q_{HT,max}$	
	$Q_{CT,max}$	Positive, scalar
	$E_{B,max}$	Positive, scalar

These variables are related with various components such as photovoltaic (PV) systems, wind turbines (WT), heat pumps (HP), and heat engines (HE). Thermal power variables encompass the production, consumption, or loss of thermal power within a given system, specifically with relation to heat pumps (HP), heat engines (HE), and the concentrated solar power (CSP) component.

Energy storage variables are used to measure the quantity of energy stored in different storage systems, such as hot and cold tanks or batteries. These variables offer valuable information about the energy that is accessible at any given moment. The On/Off Status Variables serve to identify the operational state of a particular component, so restricting the range of variation during its operation or preventing the concurrent operation of competing components such as heat pumps and heat engines. Design Variables encompass scalar variables that denote the dimensions of the primary components within the system. These variables consist of integer variables, such as the quantity of PV sub-arrays or wind turbines, as well as positive variables, including the storage capacities of TES systems, batteries, and heliostat field area.

## Overview of the Process

1. **Initial Setup:** The script starts by clearing the workspace, setting up paths to GAMS, and importing necessary Java libraries for GAMS integration.
2. **Data Preparation:** It considers weather and operational data (such as temperature, solar irradiance, and wind speed), and based on case studies, defines the electricity and thermal requirements. These requirements include irrigation pumps, light bulbs, cold rooms, refrigerators, heaters, and dryers.
3. **Energy Source Simulation:**
  - **Photovoltaics (PV):** Simulates electricity production from solar PV based on weather data and the PV system's characteristics.
  - **Wind Turbines (WT):** Simulates electricity production from wind turbines.
  - **Concentrated Solar Power (CSP/CST):** Simulates thermal energy production and losses from a CSP/CST system.
4. **Energy Storage Systems:**
  - Defines efficiencies for charging and discharging batteries.
  - Sets up a PTES system, including heat pump (HP) and heat engine (HE) parameters.
5. **GAMS Integration:**
  - Transfers simulation data to GAMS for optimization.
  - Defines parameters, sets, and scalars within a GAMS container to model the energy system's performance and economics.
6. **Optimization Variables:** Prepares arrays for storing optimization results like the number of PV strings, wind turbines, CSP output, battery and thermal storage capacities, curtailed energy demands, and system costs.

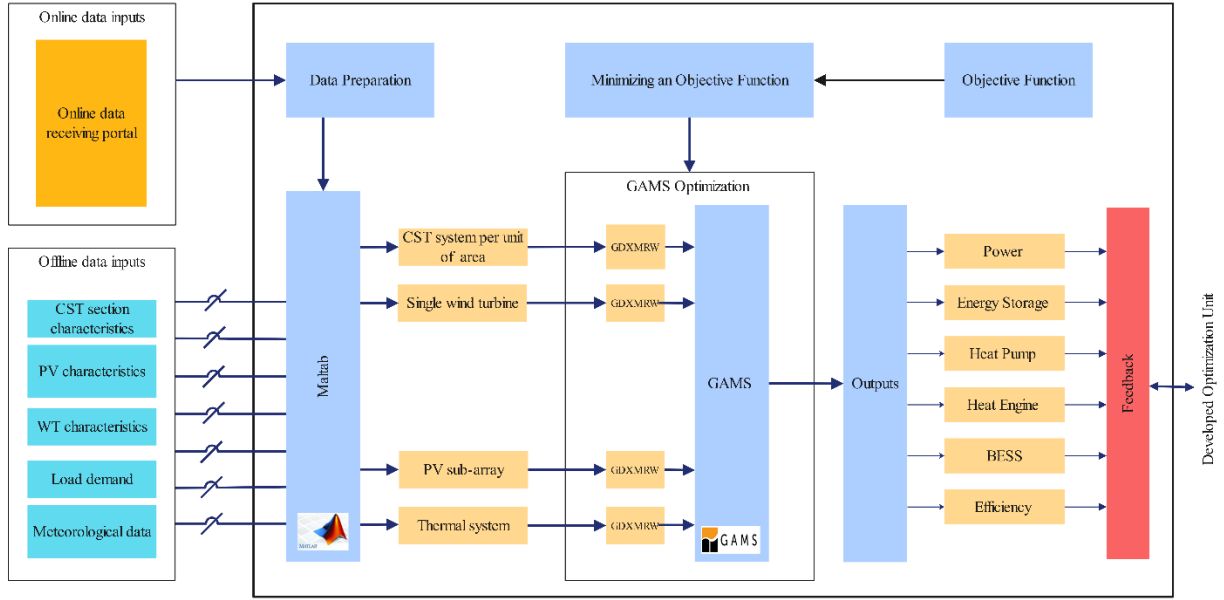


**Figure 2.** Block Diagram of Developed Optimization Unit.

#### 4. Cases Study Definitions

The given code presents a modeling framework for a PTES system, utilizing the integration of MATLAB and GAMS. The present model aims to replicate the operational characteristics of renewable energy sources, namely solar photovoltaic, wind turbines, and concentrated solar power, in conjunction with energy storage technologies such as batteries, heating and cooling thermal storage. The objective is to address diverse electricity and thermal requirements. The model that has been constructed is utilized in the analysis of the four case studies outlined in Section 1, which focuses on the preliminary design and system parameters. Table 2 displays the weather information for the sites. Data for case studies 1 to 4 has been collected over a duration of one year in order to consider the sporadic characteristics of solar and wind energy sources, which are directly impacted by geographical location. Meteororm software version 8 was utilized to acquire the meteorological data pertaining to the site being examined. The collection encompasses a diverse range of measures. The primary factors being examined include Diffuse Horizontal Irradiance (DHI), Beam Horizontal Irradiance (BHI), Wind Speed, and Ambient Temperature. The performance and potential of solar and wind energy systems in the relevant case studies are significantly influenced by these characteristics.

Figure 3 illustrates the potential of solar energy for case studies 1 to 4. It is evident that Nigerian locales exhibit a restricted seasonal fluctuation in solar radiation, in contrast to the Moroccan scenario where the daily solar irradiance during summer is roughly twice as high as that during winter. This implies that although the Moroccan instances research exhibits a greater possibility for seasonal storage, the Nigerian cases study suggests that a daily-weekly storage capacity may be adequate. Furthermore, it is worth noting that the beam irradiance weight for the Moroccan cases study exhibits a significantly greater magnitude in comparison to cases study #1 and #3. The expression of the potential of a Concentrated Solar Power (CSP) section, which exclusively

harnesses the direct component of solar radiation, may be more effectively demonstrated in the Moroccan sites. Figure 4 illustrates the distribution of wind speed at a distance of 10 meters above the ground for the four locations being examined. Nigerian case studies typically exhibit a limited wind potential, which is typical for regions near the equator. Consequently, the implementation of wind turbines is likely to be an economically unfavorable alternative. Furthermore, the wind potential of case study 2 is rather low as a result of its considerable distance from the sea. Conversely, case study #4 exhibits a significant wind potential, indicating that the implementation of wind turbines in this region could be a viable and economical option.

The box charts in Figure 5 illustrate the average trend of ambient temperature and its variance over the course of the year. It is evident that the mean temperature in Nigerian regions surpasses that of Morocco; yet, it is distinguished by diminished fluctuations in both diurnal and seasonal patterns. The performance of PV systems, wind turbines, CSP section, and heat engine performance in Rankine PTES systems is influenced by ambient temperature, assuming the usage of an air-cooler condenser. Therefore, it is anticipated that the Nigerian case study will exhibit a more consistent variation in system performance in comparison to the Moroccan example study, mostly due to fluctuations in ambient temperature.

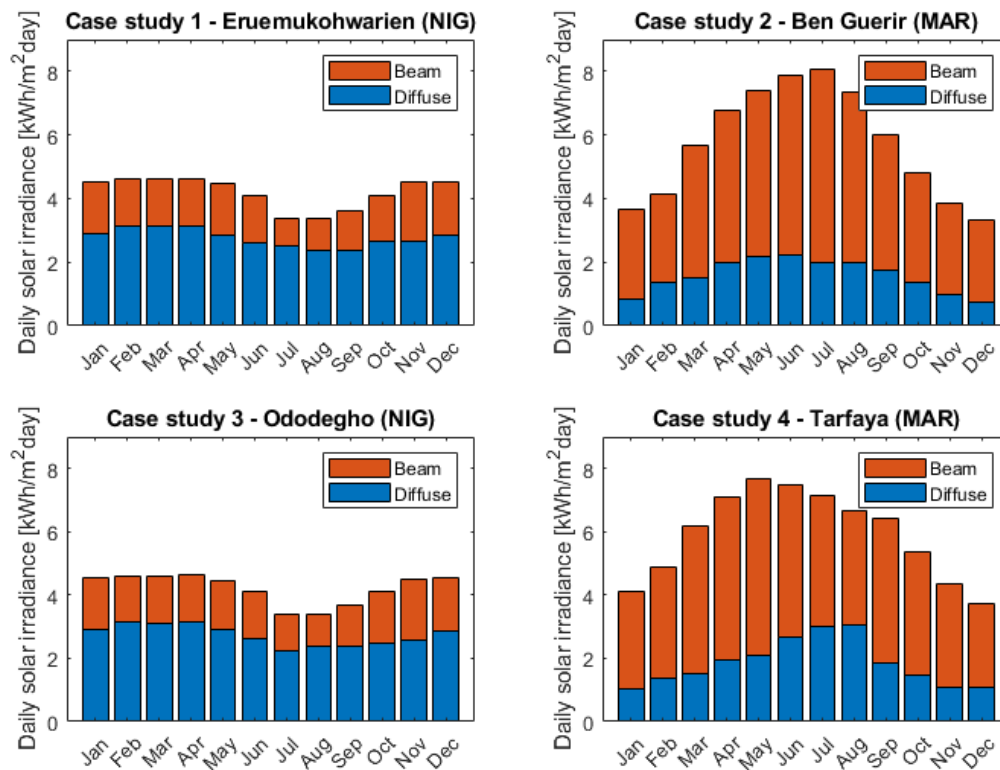


**Figure 3.** The solar radiation potential in case studies 1 to 4.

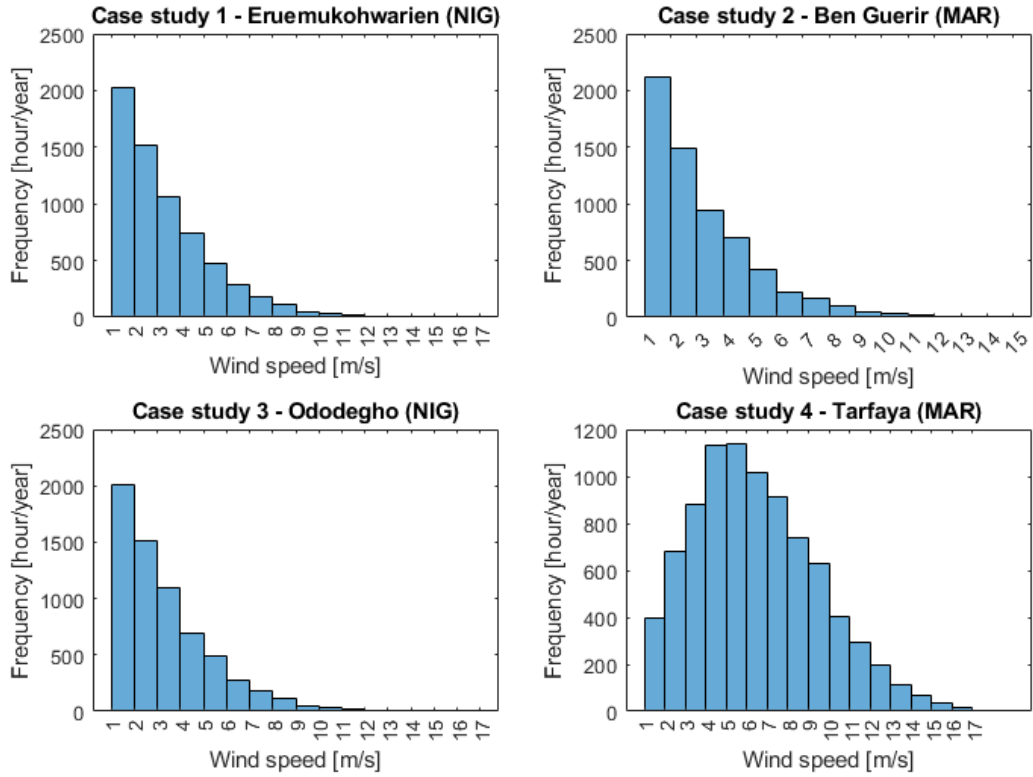


**Figure 4.** The wind energy potential in case studies 1 to 4.

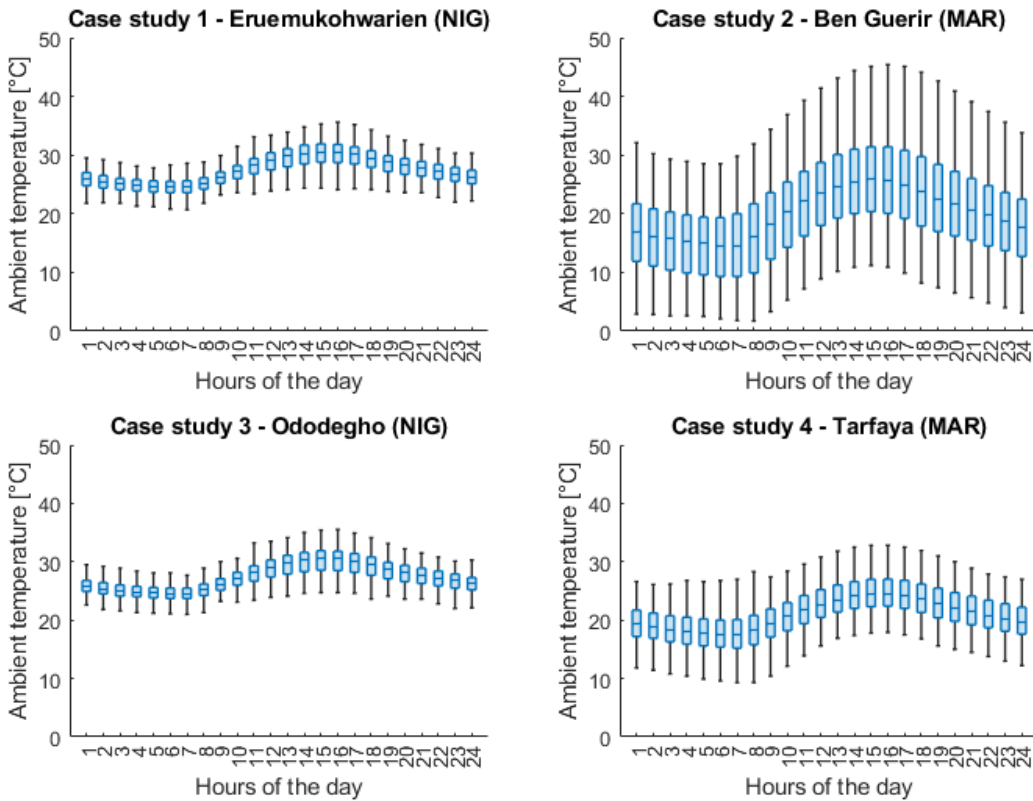


**Figure 5.** The ambient temperature in case studies 1 to 4.

**Table 2.** Site-Specific Meteorological Data.

Case Study	Location	Daily Average Global Solar Irradiance (kWh/m <sup>2</sup> ·day)	Average Wind Speed (m/s)	Average Ambient Temperature (°C)
1	Eruemukohwarien, Nigeria	4.20	2.59	27.3
2	Ben Guerir, Morocco	5.75	2.41	20.1
3	Ododegho, Nigeria	4.21	2.59	27.3
4	Tarfaya, Morocco	5.93	6.35	21.0

The load demands in terms of electrical load, cooling loads and heating loads is characterized based on the survey results outcomes reported in deliverable 1.1. In cases study 1 and 2, as illustrated in Figure 5, the RES+PTES system should be able to cover demand both in the electrical and cooling sectors. The case study 3, depicted in Figure 6, demonstrates that the system's requirements extend beyond cooling and electrical energy, including a requirement for a successful response to heat demand.

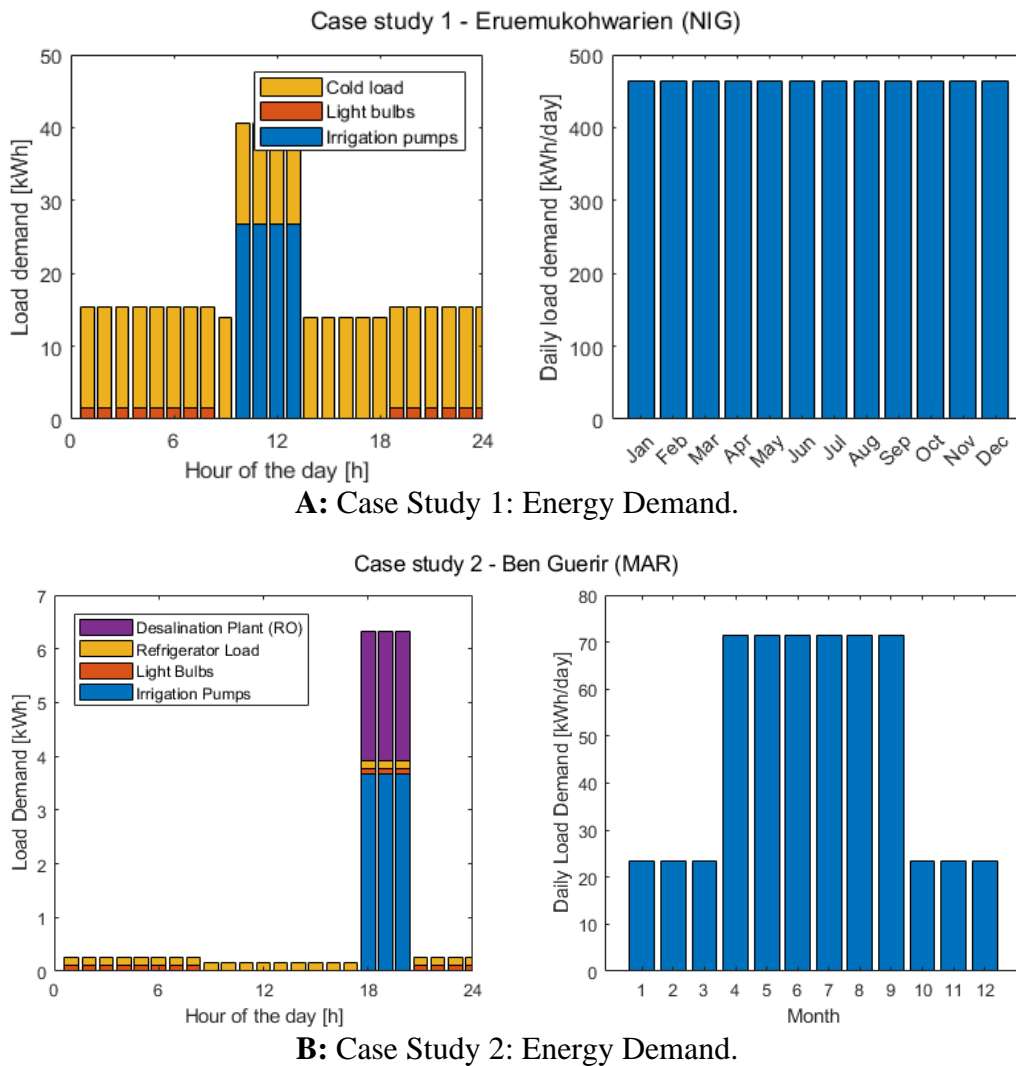


**Figure 5.** The energy demand for study cases 1 to 2.

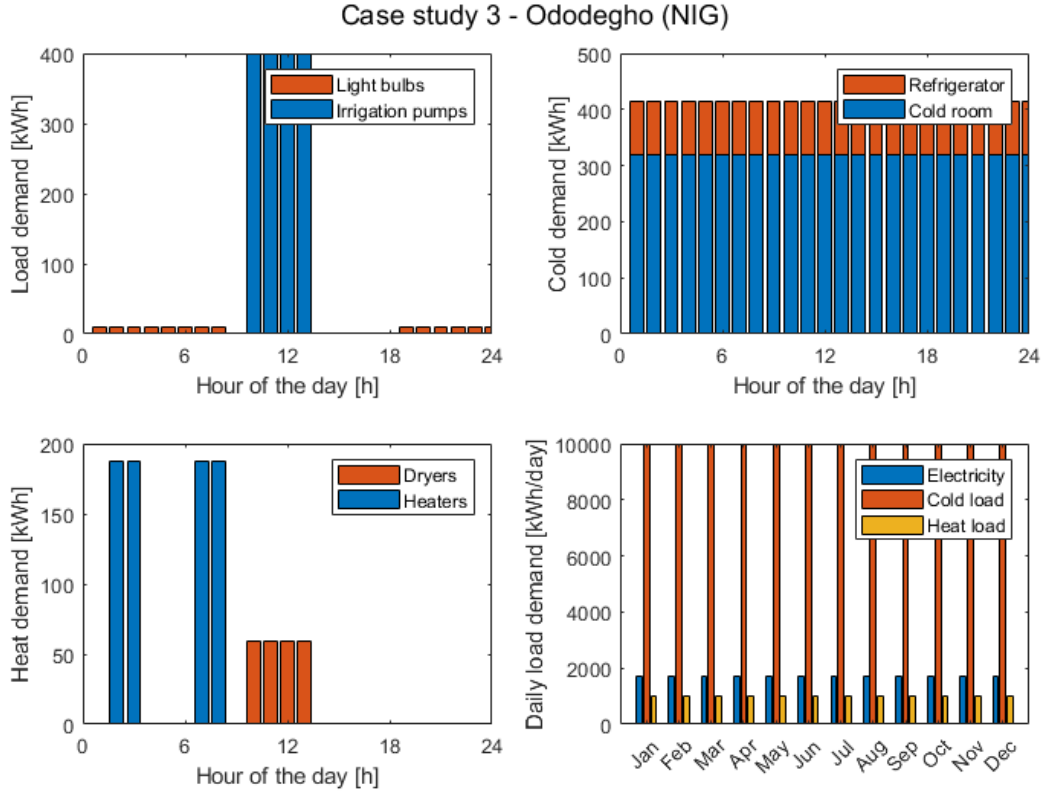


**Figure 6.** The energy demand for study cases 3.

The energy demand in case study 2 is associated with the operation of irrigation pumps, light bulbs, refrigerators, and a reverse osmosis water production plant. Table 1 presents the qualitative and quantitative attributes of water used in various areas of case study 2, as gathered from the farmers' questionnaire.

**Table 3.** The electrical conductivity (EC) range for plants and animals in Case Study 2.

Plant/Animal	EC Range (mS/cm)	Explanation
Olive tree	0.5 - 2.5	Olive trees thrive in slightly acidic to neutral soil with low to moderate salt content, and an EC level above 2.5 can hinder growth and yield.
Lemon	0.8 - 2.0	Lemons thrive in slightly acidic to neutral soil with low to moderate salt content, and an EC level above 2.0 can hinder growth and fruit production.
Orange	0.8 - 2.0	Oranges thrive in slightly acidic to neutral soil with low to moderate salt content, and an EC level above 2.0 can hinder growth and fruit production.
Pomegranate	0.5 - 2.0	Pomegranates thrive in slightly acidic to neutral soil with low to moderate salt content, and an EC level above 2.0 can hinder growth and fruit production.
Peach	0.5 - 1.5	Peaches prefer slightly acidic to neutral soil with a low salt content. An EC level above 1.5 can lead to reduced growth and fruit production.

Laying hens	< 10	High salt levels in drinking water can cause laying hens to lose water, feed, and egg production, potentially causing health issues if the EC level exceeds 10.
Rabbits	< 10	Rabbits are sensitive to high salt levels in their drinking water, which can lead to decreased water intake and dehydration, affecting their health.

The productivity factor is determined by the specific RO system and feed water quality, with a calculation for a feed water electrical conductivity of 3800-3900  $\mu\text{S}/\text{cm}$  and an irrigation flow rate of 3  $\text{m}^3/\text{h}$ . According to Ref [6], the power consumption of an RO system ( $P_{RO}$ ) can be estimated using the equation (1-29):

$$P_{RO} = \frac{\dot{Q} \times \Delta p \times \sigma}{\eta_{RO} \times R_m} \quad (1-29)$$

Where  $\dot{Q}$  is the water flow rate, measured in cubic meters per hour ( $\text{m}^3/\text{h}$ ),  $\Delta p$  indicates the pressure drop, in bars, across the RO membrane,  $\sigma$  denotes the electrical conductivity of the feed water, quantified in Siemens per centimeter ( $\text{S}/\text{cm}$ ),  $\eta_{RO}$  the efficiency of the RO system and  $R_m$  indicates the specific resistance of the RO membrane, which is assumed equal to  $10^{12} \Omega \cdot \text{cm}^2$  that is typical value for a commercial RO membrane. Table 3 suggests that an optimal value for the EC of the feed water can be around 1.5  $\text{mS}/\text{cm}$  that can be reached by combining the produced water from the RO plant with groundwater, as shown in the block diagram in Figure 7.

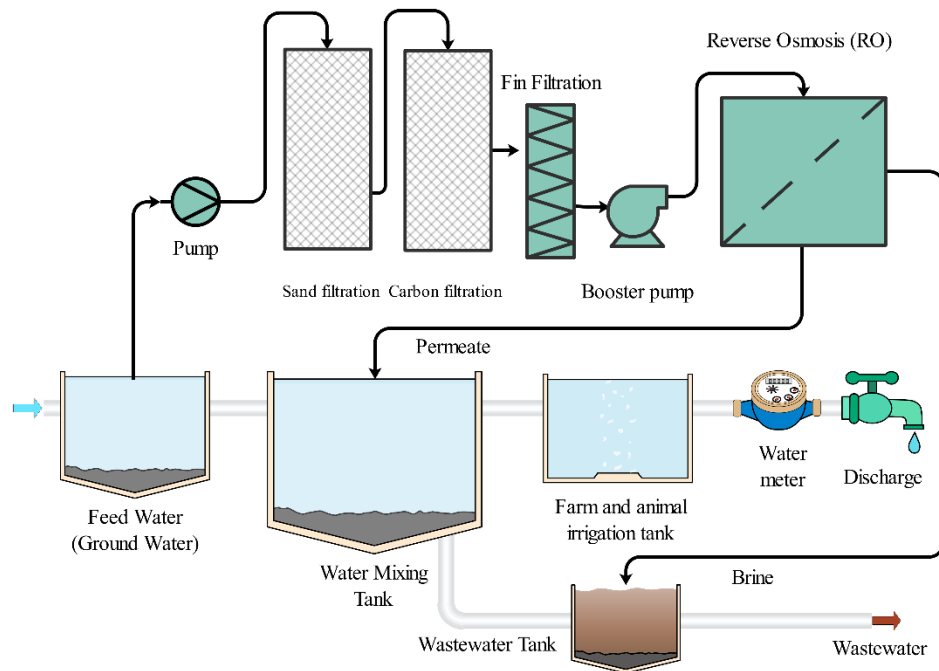


**Figure 7.** Block diagram of fresh water production plant with reverse osmosis method, case study 2.

To calculate the water flow rate to be sent to the RO, a mass balance equation is established by assigning variables for the flow rates ( $Q$ ) and electrical conductivities ( $C$ ) of each stream and the

final mixture:  $(Q_1 \times C_1) + (Q_2 \times C_2) = (Q_3 \times C_3)$ . By substituting the known values of most variables into the equation, the flow rate of the second stream ( $Q_2$ ) required to achieve the desired conductivity can be calculated. The mixing ratio is determined by dividing the value of  $Q_2$  by the total flow rate ( $Q_3$ ), which allows for accurate regulation of the resulting water quality.

By solving the equation with two variables and two unknowns, we can determine that the ideal flow rate for the RO plant in the farm water mixing tank is 1.91 m<sup>3</sup>/h, while the required flow rate from the groundwater source to the mixing tank is 1.09 m<sup>3</sup>/h. By employing the provided specifications, we can replace the given values into the appropriate parameters. The assumed pressure drop across the RO membrane ( $\Delta p$ ) is 20 bars, the electrical conductivity of the feed water ( $\sigma$ ) is 0.039 S/cm, and the efficiency ( $\eta_{RO}$ ) of the RO system is 60%. The power consumption of the RO system is estimated to be approximately 2.4 kW.

## RESULTS

In this section, the preliminary design of a RES+PTES system devoted to cover the energy demands of the four cases analysed is presented and discussed. Obviously, the optimal design of such system configuration is strongly influenced by the meteorological characteristics of the site in which the cases study are located. Specifically, case study 1 conducted in Eruemukohwarien indicates substantial solar energy potential, despite the presence of moderate wind speeds and high ambient temperatures. The daily sun irradiation is 4.20 kWh/m<sup>2</sup>, the average temperature is 27.3°C, and the wind speed is 2.59 m/s. In the fourth case study conducted in Tarfaya, it was shown that increased sun irradiance (5.93 kWh/m<sup>2</sup>/day), lower average temperatures (21°C), and higher wind speeds (6.35 m/s) have the potential to enhance the efficiency of solar panels by means of cooling effects. However, these factors may also provide difficulties for wind-sensitive infrastructure. The environmental conditions of these places play a crucial role in assessing the suitability of PTES system for meeting local energy demands, namely in the areas of heating and cooling. Owing to the absence of heating requirements and the expected power and energy capacity requested to the PTES system, a reversible Rankine configuration is chosen for the PTES system for case studies 1 and 2. In contrast, case study 3 and 4 utilized a Brayton configuration to accommodate both electrical, heating and cooling loads.

**Table 4.** Assumed values for the main parameters used in the system modelling.

Subsystem	Parameter	Value	Reference
<i>PV system</i>	Type	PV-MJT250GB	[7]
	$P_{PV,s,nom}$	10 kW	
	$\alpha_p$	-0.45%/K	
	NOCT	47°C	
<i>Wind turbine</i>	Type	NPS 100C-24	[8]
	$P_{WT,nom}$	100 kW	
	$k_w$	0.05	
	$k_{aux}$	0.02	

<i>CSP plant</i>	$\eta_{opt}$	0.65	[9,10]
	$A_{rec}$	5.94 m <sup>2</sup>	
	$\varepsilon_{rec}$	0.1	
	$U_L$	5 W/m <sup>2</sup> K	
<i>PTES system</i>	$P_{HP_{nom}}$	Variable	
	$P_{HP_{min}}$	0.2 $P_{HP_{nom}}$	
		1.5831 (Rankine type, Case study #1)	
	COP	--- (Rankine type, Case study #2)	
		--- (Brayton type, Case study #3)	
		--- (Brayton type, Case study #4)	
	$P_{HE_{nom}}$	max ( $P_L$ )	
	$P_{HE_{min}}$	0.4 $P_{HE_{nom}}$	
	0.0381 (Rankine type, Case study #1)		
	--- (Rankine type, Case study #2)		
	--- (Brayton type, Case study #3)		
	--- (Brayton type, Case study #4)		
<i>BESS</i>	$\eta_{BC}$	0.95	
	$\eta_{BD}$	0.95	
<i>Specific costs</i>	$C_{PV}$	10 k\$/subarray	[11]
	$C_{WT}$	500 k\$/turbine	[12]
	$C_{HF}$	800 \$/m <sup>2</sup>	[13]
	$C_{TES}$	100 \$/kWh	[14]
	$C_B$	2000 \$/kWh	[11]

In the following, the main results obtained by the optimization procedure described in the previous sections will be introduced for each case study. Two different scenarios will be analysed: the optimal design of a RES+PTES system able to completely covered the load demand will be investigated as first scenario, while a second scenario will assess the variation in the system configuration and sizing with increasing percentages of allowed load curtailment. Table 4 reports the value imposed for the main parameters in the developed modelling.

## 1. Cases Study #1

### 1.1 Complete satisfaction of the load demand

The optimal design of the RES+PTES system obtained for Case Study 1 and the corresponding expected annual performance is presented for different power ratios ( $P_r$ ) between the heat pump and heat engine. The nominal power of the heat engine, which represents the power output of the Rankine PTES system during the discharging phase, was established as being equal to the peak

electrical load, based on a fundamental assumption. The manipulated parameter was the nominal power of the heat pump, which represents the power consumed by the Rankine PTES system during the charging phase. Figure 8 shows the variation of the objective function, which is representative of the expected system costs, for different values of  $P_r$ . The obtained results suggests that to sufficiently meet the energy requirements, it is necessary for the nominal power of the heat pump to be at least 50% more than that of the heat engine. Additionally, it was noticed that the performance of the system was improved by increasing the nominal power of the heat pump to 2.5-2.75 times that of the heat engine. Further increments over this threshold led to slight enhancements but also caused higher beginning expenses. Table 5 provides additional information regarding the design values of various components of the RES-PTES system. These components include the PV system, wind turbine, CSP system, as well as heat pump, heat engine, hot and cold tank storage capacities and battery storage capacity

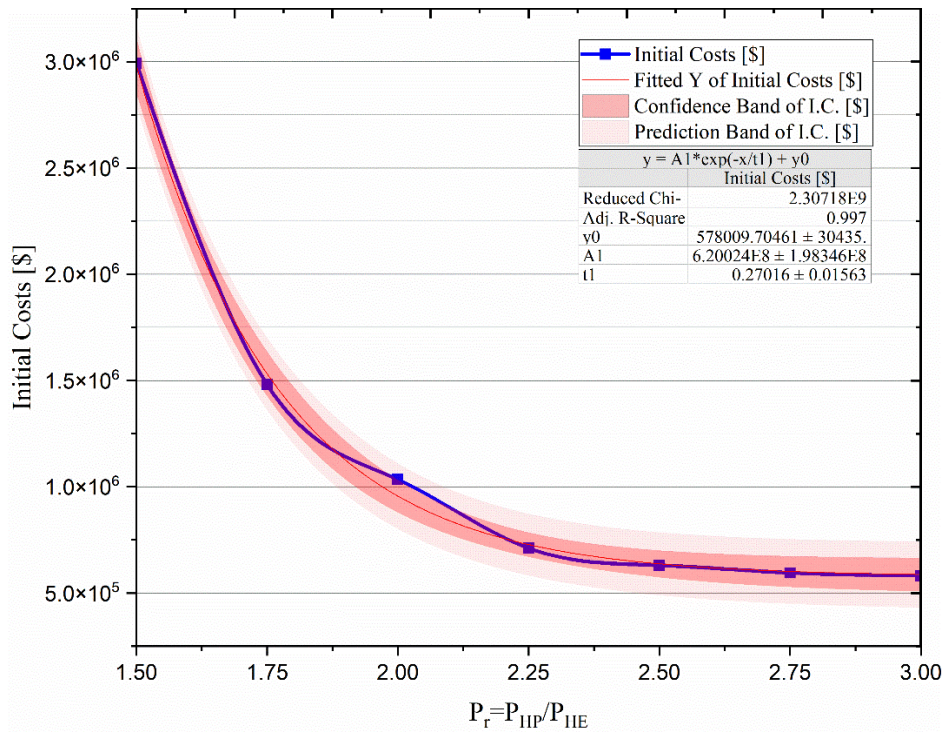


**Figure 8.** Comparing the minimum values obtained for initial costs with various power ratios ( $P_r$ ) of system.

**Table 5.** Sizing of the RES-PTES system by varying the heat pump rated power.

Design Parameter	U.o.M.	$P_r$ = Heat pump rated power / Heat engine rated power						
		$P_r=1.5$	$P_r=1.75$	$P_r=2$	$P_r=2.25$	$P_r=2.5$	$P_r=2.75$	$P_r=3$
$n_s$	[-]	41	51	31	48	41	37	38
$n_{WT}$	[-]	4	1	1	0	0	0	0
$A_{HF}$	[m <sup>2</sup> ]	0	0	0	0	0	0	0
$P_{HP,nom}$	[kW]	40.0	46.7	53.4	60.0	66.7	73.4	80.0
$P_{HE,nom}$	[kW]	26.7	26.7	26.7	26.7	26.7	26.7	26.7
$Q_{HT,max}$	[kWh]	1445.2	1268.2	976.9	1039.9	1092.9	1135.6	854.7

$Q_{CT,max}$	[kWh]	4193.9	3123.9	1018.5	931.1	852.6	879.9	822.9
$E_{B,max}$	[kWh]	9.2	15.5	12.3	16.9	12.7	11.6	17.1

As reported in the table, the low direct solar irradiance of the Nigerian site penalizes the use of concentrating solar technologies and its use is therefore not recommended. An important variation in the RES-based system configuration is observed by varying the parameter  $P_r$ : for  $P_r \leq 2$ , the minimization of the objective function is obtained by a hybrid PV+WT configuration, while for heat pump rated power higher than this threshold the installation of only PV system is suggested. A low heat pump rated power would require a power supply even during night to satisfy cold loads that could be given only by WT, while with an increase in heat pump sizing, a better exploitation of solar energy is achieved, with the consequent preference of a PV-only configuration.

The change in RES generator configuration also affect the required storage capacities. The needed capacity in the storage is depicted in Figure 9. When the value of  $P_r$  is increased, there is a significant decrease in the required capacity in both tanks, with a steep slope, until  $P_r$  reaches 2. At this point, the demand to increase the capacity in the cold tank is significantly greater than that in the hot tank, approximately two times or more. However, when  $P_r$  is equal to 2, the rate of increase becomes similar. The hot and cold tanks have been in touch at two specific points, denoted as  $P_r = 2$  and 3. Hence, it appears that the change from a hybrid WT+PV configuration to a only PV configuration results in a marginal impact of  $P_r$  in the dimensions of the cold and hot tank, nor does it have a substantial effect on the cost function of the entire system (Figure 8). The battery energy storage system (BESS) exhibits an almost constant storage capacity and the effect  $P_r$  in this design parameter is marginal.

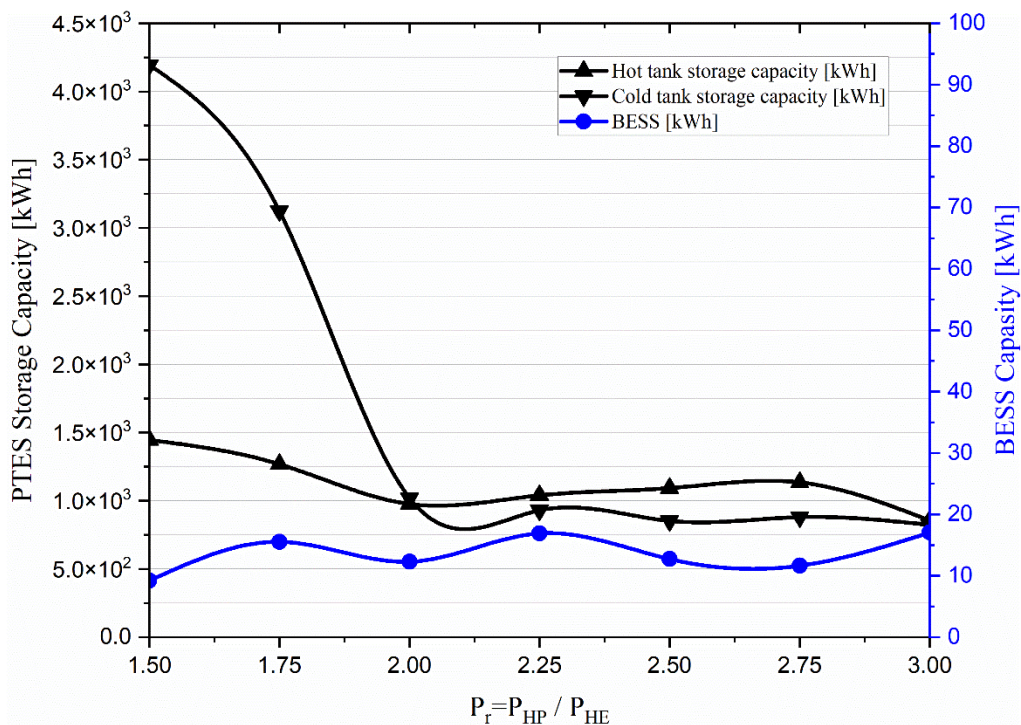


**Figure 9.** The required capacity in the storage with various power ratios ( $P_r$ ) of system.

The annual electrical production of the RES-based generators is depicted in Figure 10, measured in terms of  $P_r$ . The system's efficiency exhibits an exponential relationship, with the highest production observed at  $P_r=1.5$  and the lowest at  $P_r=3$ . It can be observed a discontinuity in the trend when moving from a WT+PV configuration to a PV-only configuration. The optimal equation for the annual production of renewable energy in single source mode is represented by equation (1-30); in the hybrid zone, which represents production from two solar and wind sources, it is represented by equation (1-31). In equation (1-30) the Reduced Chi-Square value of 344.328 indicates an excellent fit of the model to the data. The value of Adj. R-Square, 0.922, signifies that the independent variables explain most of the variation in the dependent variable. The elevated value of 0.922 confirms the aptness of the model for explaining the observed data. Additionally, the initial value of the calculated model in study case 1,  $y_0$ , is  $497.509 \pm 23.876$ . The value of  $A_1$ , which is  $4432760.465 \pm 2.446e7$ , implies a substantial influence of the independent variable on the dependent one. The rate of change in the dependent variable in response to the independent variable is represented by  $t_1$ , which is estimated to be  $0.218 \pm 0.119$ .

$$y = A_1 \times e^{\left(\frac{-x}{t_1}\right)} + y_0 \quad (1-30)$$

$$y = A \times e^{(R_0 \cdot x)} + y_0 \quad (1-31)$$

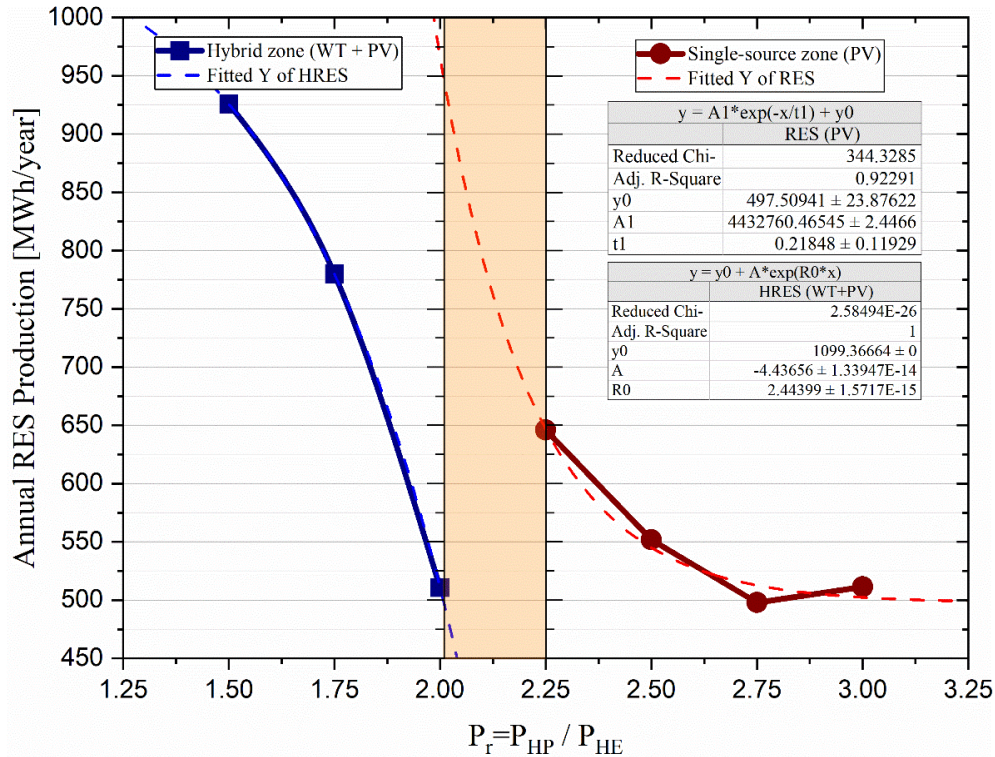


**Figure 10.** The annual RES production with various power ratios ( $P_r$ ) of system.

The Curtailed Energy of the system is depicted in Figure 11. Additionally, this figure illustrates the extent to which the system can harness the potential of renewable energy sources, a factor that was not taken into account in the case study 1. The equation (1-32) is crucial in establishing the ideal

curtailed energy, which represents the renewable energy generated but not consumed or stored, within the context of maximizing the usage of renewable energy systems. The equation, as depicted in Figure 11, exhibits a Adj. R-Square value of 0.862 in the single source zone, suggesting a strong alignment between the model and the observed data. This shows that a substantial amount of the differences in the curtailed energy can be explained by the model. The equation comprises multiple elements: 'y' denotes the curtailed energy, 'y<sub>0</sub>' represents the offset constant, 'A' signifies the amplitude of the curtailed energy potential, 'R<sub>0</sub>' represents the decay rate, and 'x' represents the independent variable, which may be time or another system parameter that influences energy curtailment. The exponential function's existence signifies that alterations in the system parameter 'x' result in a multiplicative impact on the curtailed energy. As the value of x increases significantly, the minimum value of y tends to approach, under the assumption that R<sub>0</sub> is negative. Conversely, the maximum value of y is dictated by the sum of 'y<sub>0</sub>' and 'A', which happens when 'x' reaches its minimum value. The integration of consumer energy systems, such as green ammonia production or desalination facilities, relies heavily on this relationship. These systems can utilize surplus renewable energy, which would otherwise be squandered.

$$y = A \cdot e^{R_0 \cdot x} + y_0 \quad (1-32)$$

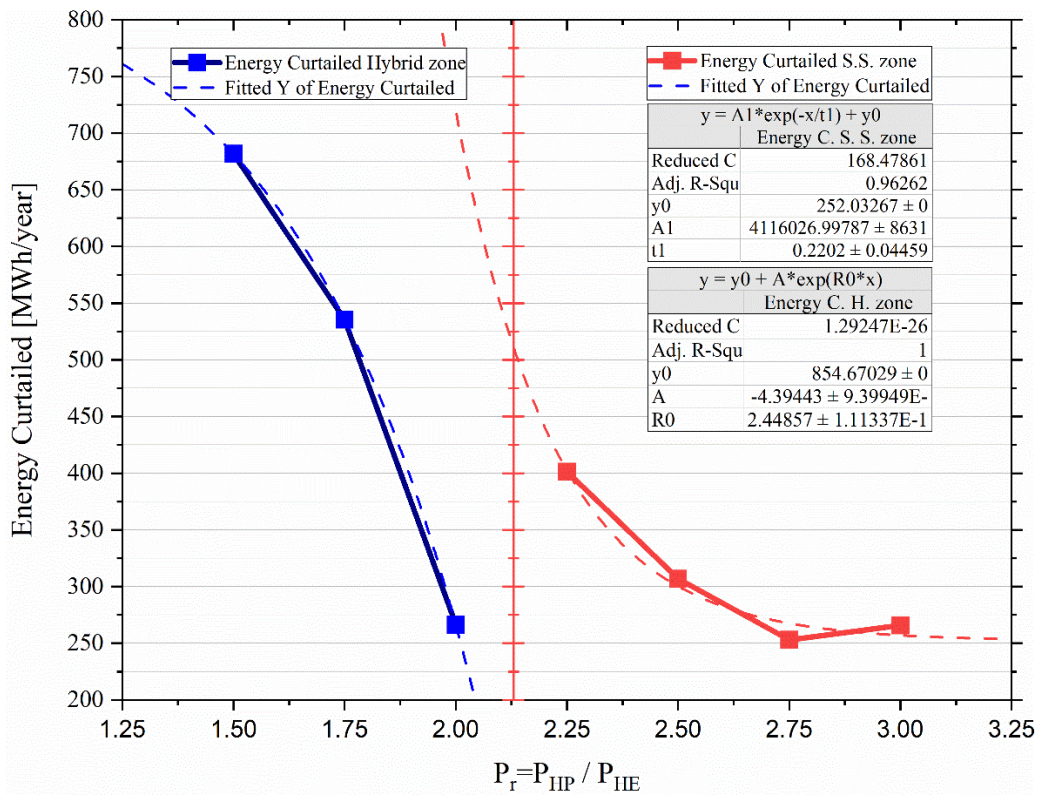


**Figure 11.** The energy curtailed with various power ratios ( $P_r$ ) of system.

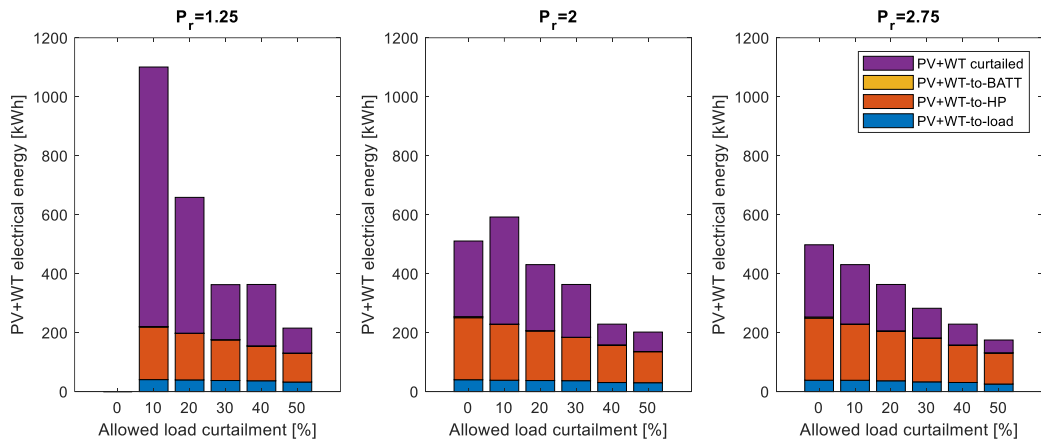
The parameters of the exponential decay model are determined by equation (1-32). In this equation,  $y_0$  is defined as 252.032 in single source zone, which represents the asymptotic value of  $y$  as  $x$  increases. There is no reported uncertainty associated with  $y_0$ , indicating that it is considered a fixed value in this context. Similarly,  $A_1$  is defined as 4116026.997, which represents the initial

difference from  $y_0$  when  $x$  is zero.  $A_1$  is reported with an uncertainty of  $\pm 8631450.012$ , making it a variable value in the analysis. The  $t_1$  value is 0.220, representing the decay constant. This constant has an associated uncertainty of  $\pm 0.044$ . It indicates the rate at which  $y$  drops as  $x$  grows. The statistical metrics presented in this study confirm the adequacy of the model's fit to the data. The Reduced Chi-Squared value of 168.478 indicates that the model is well-fitted to the data, considering the degrees of freedom. The Adjusted R-Square value of 0.962 also confirms the model's goodness of fit. Additionally, the Adjusted R-Square value of 0.862 suggests that approximately 86.276% of the variance in Curtailed Energy can be accounted for by the model. This value is considered to be a highly satisfactory fit.

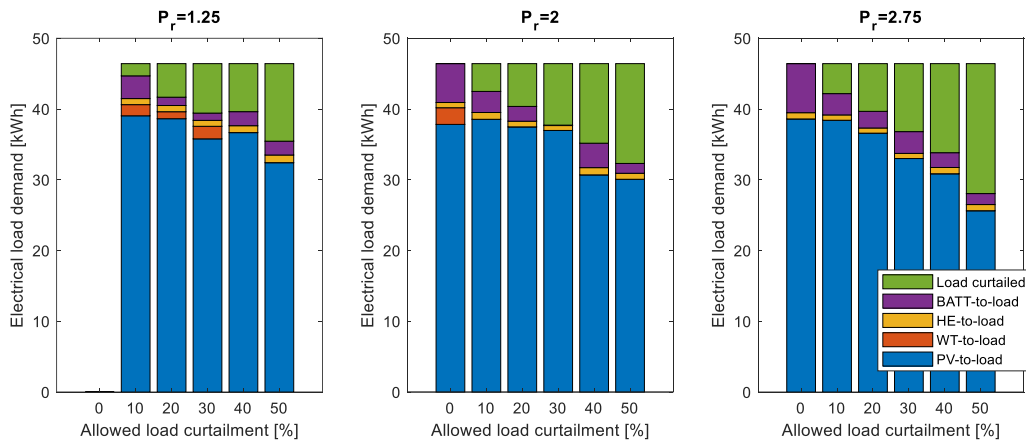
### *1.2 Effect of the allowed load curtailment*

The comparison of Figure 10 with Figure 11 reveals that, even with an optimized heat pump rated power, more than 50% of the energy produced by RES generator is curtailed. This oversizing is mainly due to the strong constraint of completely satisfy the electrical and cold demands during the year. Furthermore, the optimization process reveals that the large cold energy request demands a heat pump sizing at least 50% more the heat engine rated power. In this section, the effect of allowing a daily percentage of load curtailment in the system design and corresponding performance is investigated.

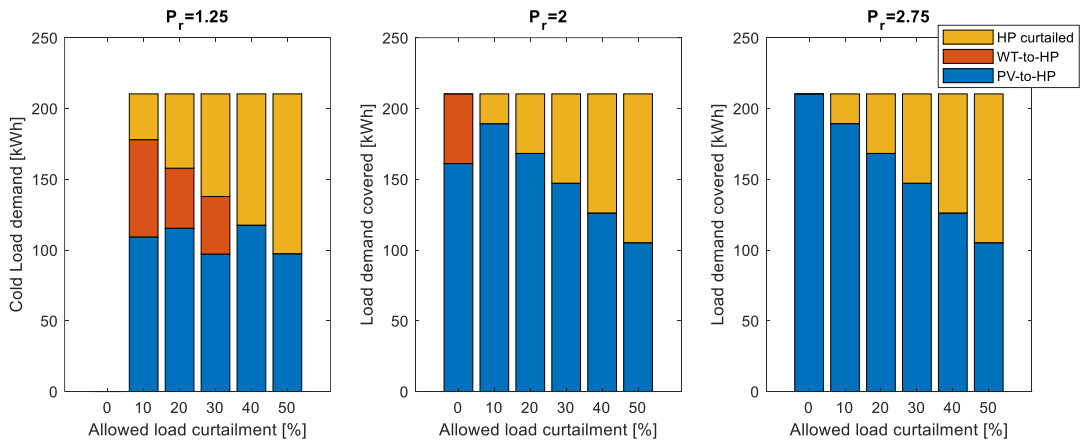
Figure 12 displays the yearly distribution of energy allocation for the various energy supply sources, such as photovoltaic power plants and wind power plants, based on  $P_r$  under different conditions of allowed load curtailment. Figure 10A comprises three subplots showing the use of electrical energy generated by RES systems at various pump ratios. The x-axis in both subplots reflects the permitted reduction in load as a percentage, while the y-axis indicates the total electrical energy generated by photovoltaic and wind turbine systems in kilowatt-hours (kWh). The blue section of each bar represents the energy directly provided to the load, the red section indicates the energy provided to the heat pump (HP), the yellow section relates to the energy provided to the battery (BESS), and the violet section represents the energy that is not used and is thus wasted. As can be observed, the solution with a  $P_r=1.25$  becomes feasible if at least a 10% of load curtailment is allowed. In any case, this solution leads to a great oversizing of the RES systems with a large use of energy curtailment. In general, the increase of the allowed load curtailment results in a corresponding reduction of the energy curtailment, with the exception of some cases (such as a load curtailment of 40% for a  $P_r = 1.25$  or a load curtailment of 10% for a  $P_r=2$ ) characterized by a change in the system configuration from a hybrid PV+WT solution to a PV only one. Moreover, as already observed in Figure 9, the curtailment energy reduced as the  $P_r$  value increased but this benefits becomes increasingly marginal with the rise of the allowed load curtailment.



**A:** Comparison of Electrical Energy Production of RES for Different of System  $P_r$ .



**B:** Electrical Load Demand Distribution for Different of System  $P_r$ .



**C:** Cold Load Demand Coverage for Different of System  $P_r$ .

**Figure 12.** Annual energy generated by the RES source and utilized in subsystems under varying allowed load curtailment conditions.

Figure 12B and 12C display the distribution of electrical load demand and cold load demand, respectively, for different levels of load curtailment, expressed as a percentage. The electrical load is mainly covered by PV system, while WT energy production, when present, is used to partially supply heat pump for covering cold load demand. The role of heat engine, which is characterized by a low efficiency, is rather marginal compared to batteries for all the cases analyzed. Furthermore, the actual share of electrical load curtailment for a given allowed percentage is not constant with the change of  $P_r$ , unlike that observed for the cold load curtailment. This reveals that Eq. (1-26) is a weak constraint compared to Eq. (1-27), and the design of the RES-PTES system is mainly aimed at meeting the cold load demand.

Figure 13 illustrates the change in the restriction for managing the permissible level of unfulfilled energy by setting a specific percentage of the daily load demand that can be not satisfied, with varying values of  $P_r$ . The investigation suggests that in order to meet energy requirements effectively, it is essential for the nominal power of the heat pump to be higher than that of the heat engine by a factor ranging from 1.25 to 2.75. As depicted in the diagram, enhancing the heat pump's capacity to twice that of the heat engine results in an enhancement of the system's performance. However, this increase has a significantly smaller gradient compared to the previous value of 2. Changing  $P_r$  above the threshold of 2.5 will not significantly impact the initial cost of the system, despite the associated rise in design expenses. However, additional increases beyond this point provide minimal advantages but lead to higher initial costs. The investigation conducted in Figure 13 pertains to the proportions of allowed load curtailment ranging from 0% to 50%. An exponential equation, such as Equation 1-30, provides the most precise fit for the desired function. This equation incorporates constant values for each allowed load curtailment value. The equations for fitting are depicted in Figure 12, represented by a dashed line together with its corresponding function.

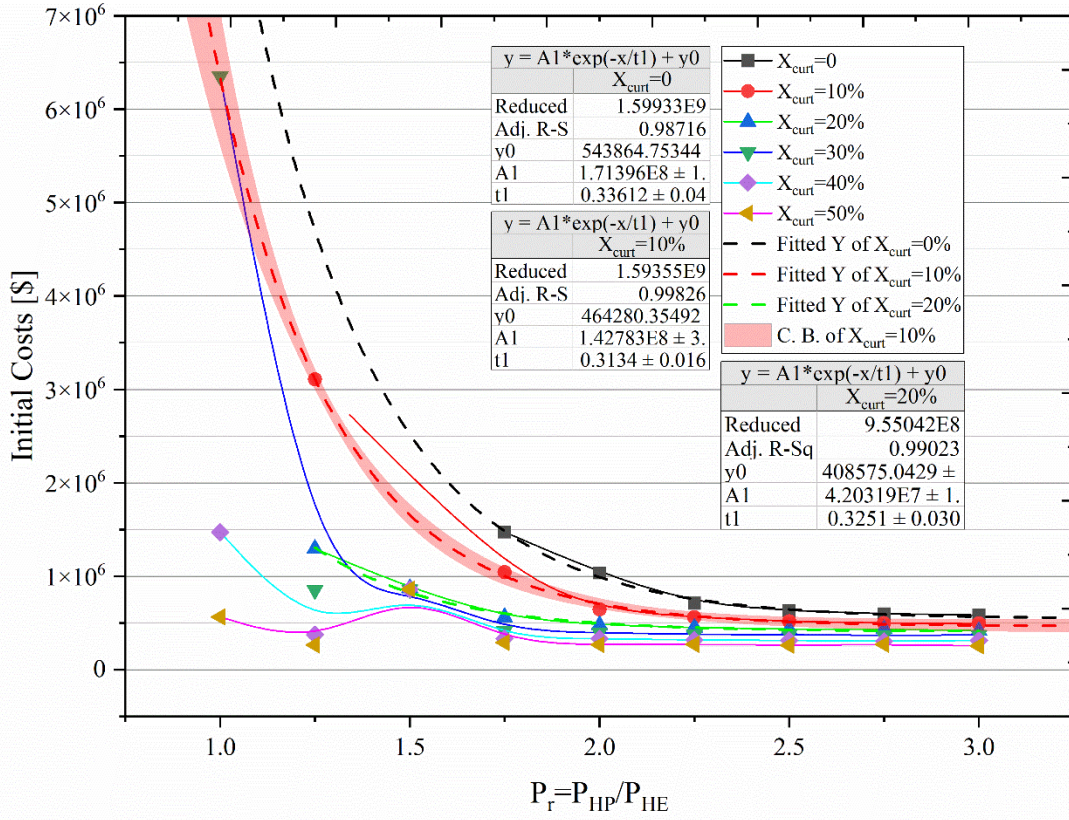


**Figure 13.** The impact of  $P_r$  on the allowed load curtailment of system.

In practical applications, the utilization of this equation enables strategic decision-making regarding the sale of surplus electricity to the grid or its allocation to peripheral systems that can optimize its utilization. For example, in situations when the model predicts a significant reduction in energy supply, operators have the option to increase the production of green ammonia, a process that requires a substantial amount of energy, in order to capitalize on the existing renewable energy resources. The utilization of this intelligent energy management strategy not only improves the overall effectiveness but also enhances the sustainability of these systems by incorporating renewable energy sources. As a result, it promotes the production of environmentally friendly commodities such as ammonia without dependence on fossil fuels.

### 1.3 Proposed system configuration

Based on the results obtained from the preliminary design analysis and the indications that emerged from the survey conducted on the small farm, specifically:

- Energy availability from the national grid: Readily available (40%), Scarcely available (60%)
- Available land allocated for renewable energy installations: 1 hectare
- Prospects of Higher Power Demand: a moderate increase in power demand in the next 3 years (25% - 75%).

Table 6 presents the proposed configuration of the system, which is as follows:

**Table 6.** Proposed design of the RES-PTES system

Configuration	Parameter	Description	Value
<b>RES</b>	Nominal Power	Rated output power of the PV system	250 kW
	Tilt/Azimuth Angle	Tilt and orientation angles of PV modules	10°/0°
	Total Module Area	Estimated area occupied by PV modules	1250-1350 m <sup>2</sup>
	Land Area	Estimated land area required for the PV system	0.7-0.8 hectares
<b>PTES</b>	Heat Pump Power	Rated power of the heat pump	70 kW
	Heat Engine Power	Rated power of the heat engine	26 kW
	Hot Tank Capacity	Thermal energy storage capacity of the hot tank	800 kWh
	Cold Tank Capacity	Thermal energy storage capacity of the cold tank	800 kWh
<b>BESS</b>	Charging/Discharging Power	Rated power for charging and discharging the battery	26 kW
	Storage Capacity	Total energy storage capacity of the battery	26 kWh

The proposed configuration, outlined in Table 6, comprises a 250 kW photovoltaic system, a PTES system with a 70 kW heat pump and a 26 kW heat engine, and a BESS with a 26 kW charging/discharging power and a 26 kWh storage capacity. This configuration is expected to meet around 80-90% of the load demands. This structure would allow the farm to function independently, reducing the burden of limited electricity availability from the national grid. The PV system, with an estimated total module size ranging from 1250 m<sup>2</sup> to 1350 m<sup>2</sup> and a land area need of 0.7 to 0.8 hectares, is projected to generate roughly 300 to 350 megawatt-hours per year. However, given the existing demand for electricity, it is expected that approximately 30-35% of the energy produced will have to be reduced or restricted. However, considering the anticipated rise in power consumption in the future, this energy restriction can be lessened by employing a portion of the excess energy. Moreover, while the optimization procedure suggests a restricted optimal battery storage capacity, it is recommended to build a BESS with enough storage capacity to meet the peak load demand for one hour. This BESS would assist in mitigating fluctuations in output within an hour or unanticipated demands for electricity, so guaranteeing a more consistent and dependable energy provision.

## CONCLUSION

This report presents the equations and their application in optimizing multiple design parameters for an advanced energy system. The study encompasses PV sub-arrays, wind turbines, a CSP plant, and a BESS. The optimization of PV sub-array systems primarily focuses on the number of sub-arrays, whereas in a CSP plant, the mirror area is the key parameter to optimize. The nominal power, global irradiation, temperature coefficient of power, and cell temperature determine the power output of the PV sub-array system. The total power generation of the PV system is determined by taking into account the power output of each PV sub-array, the efficiency of the inverter, the PV derating factor, and the number of integrated sub-arrays. The wind turbine power

output is determined by applying a four-dimensional equation to the hub wind speed. The power generated by the wind farm is determined by various factors, including the power output of each wind turbine, the ratio of hub density to reference density, the auxiliary loss factor, the wake factor, and the total number of wind turbines. The study used mathematical equations, MATLAB, and GAMS to model the systems. Equations were employed to determine under different conditions. Conditions were additionally established to ensure that power and heat outputs remained within specified limits. According to the analysis, hot and cold thermal storage systems enhance the efficiency and reliability of renewable energy systems. These storage devices are crucial for the storage of energy, the management of loads, and the reduction of peak demand.

According to the design, in order to meet the energy requirements, the heat pump should have a nominal power that is at least 50% higher than that of the heat engine. Additionally, raising the notional power of the heat pump to 2.5 times that of the heat engine improves the performance of the system. The model demonstrates a strong alignment between the observed data and the model, as evidenced by its high Adjusted R-Square value of 0.8627. The parameters of the equation, such as the asymptotic value ( $y_0$ ), the amplitude ( $A$ ), and the decay rate ( $R_0$ ), are obtained by statistical analysis and offer useful insights for making strategic decisions about the use of excess renewable energy. The key findings of the study reveal that there is an ideal power ratio ( $P_r$ ) between the heat pump and heat engine that results in the most cost-effective system. Additionally, the study proposes a model for maximizing the amount of curtailed energy. The suggested RES-PTES combination, comprising a 250 kW photovoltaic system, a 70 kW heat pump, a 26 kW heat engine, and a 26 kW/26 kWh BESS, is anticipated to fulfill 80-90% of the required energy. An analysis was conducted to assess the effects of permitted load curtailment. The findings indicate that as curtailment increases, the amount of energy that is curtailed decreases. It is recommended to size the heat pump between 1.25 and 2.75 times the power of the heat engine. An exponential equation precisely models the correlation between the amount of load curtailment that is permitted and the initial cost of the system. The proposed system consists of a 250 kW photovoltaic system, a 70 kW heat pump, a 26 kW heat engine, and a 26 kW/26 kWh BESS, based on preliminary design and data from surveys from the farm. The PV system, covering an area of 1250-1350 square meters or 0.7-0.8 hectares, is intended to generate an annual energy output of 300-350 megawatt-hours (MWh). Approximately 30-35% of the generated energy will be curtailed to match the current demand. Considering the possibility of a 25-75% rise in power demand, it is advisable for the BESS to store enough energy to meet one hour of peak load in order to maintain a stable energy supply.

## REFERENCES

- [1] L. Migliari, M. Petrollese, G. Cau, D. Cocco, Techno-economic assessment and grid impact of Thermally-Integrated Pumped Thermal Energy Storage (TI-PTES) systems coupled with photovoltaic plants for small-scale applications, *J. Energy Storage*. 77 (2024) 109898. <https://doi.org/10.1016/J.EST.2023.109898>.
- [2] A. Ghilardi, A. Baccioli, G.F. Frate, M. Volpe, L. Ferrari, Integration of ocean thermal energy conversion and pumped thermal energy storage: system design, off-design and LCOS evaluation, *Appl. Therm. Eng.* 236 (2024) 121551. <https://doi.org/10.1016/J.APPLTHERMALENG.2023.121551>.

- [3] P. Wang, Q. Li, S. Wang, C. He, C. Wu, Off-design performance evaluation of thermally integrated pumped thermal electricity storage systems with solar energy, *Energy Convers. Manag.* 301 (2024) 118001. <https://doi.org/10.1016/J.ENCONMAN.2023.118001>.
- [4] X. An, Q. He, Q. Zhang, R. Liu, C. Lu, D. Du, Physical modeling and dynamic characteristics of pumped thermal energy storage system, *Energy*. 290 (2024) 130144. <https://doi.org/10.1016/J.ENERGY.2023.130144>.
- [5] B. Kurşun, K. Ökten, B. Özak, Reducing the cost of electricity storage with a novel solar thermal support scenario in pumped thermal energy storage (PTES), *Appl. Therm. Eng.* 241 (2024) 122317. <https://doi.org/10.1016/J.APPLTHERMALENG.2023.122317>.
- [6] DuPont™, Water solutions: FilmTec™ Reverse Osmosis Membranes Technical Manual, Costa Brava Region, Spain, 2020. <https://www.dupont.com/content/dam/dupont/amer/us/en/water-solutions/public/documents/en/RO-NF-FilmTec-Manual-45-D01504-en.pdf>.
- [7] MJT-GB, MJT-GB-Series Datasheet (en), Ratingen, 2024. [https://www.mitsubishi-pv.de/index-service\\_en.php](https://www.mitsubishi-pv.de/index-service_en.php).
- [8] Northern Power Systems, NPS 100C-24 Class III/A, Barre, Vermont, 2024. <https://windup.pt/resources/Brochure NPS 100-24.pdf>.
- [9] R.P. Merchán, M.J. Santos, I. Reyes-Ramírez, A. Medina, A. Calvo Hernández, Modeling hybrid solar gas-turbine power plants: Thermodynamic projection of annual performance and emissions, *Energy Convers. Manag.* 134 (2017) 314–326. <https://doi.org/10.1016/J.ENCONMAN.2016.12.044>.
- [10] R.P. Merchán, M.J. Santos, J. García-Ferrero, A. Medina, A.C. Hernández, Thermo-economic and sensitivity analysis of a central tower hybrid Brayton solar power plant, *Appl. Therm. Eng.* 186 (2021) 116454. <https://doi.org/10.1016/J.APPLTHERMALENG.2020.116454>.
- [11] R.P. Micena, O.R. Llerena-Pizarro, T.M. de Souza, J.L. Silveira, Solar-powered Hydrogen Refueling Stations: A techno-economic analysis, *Int. J. Hydrogen Energy*. 45 (2020) 2308–2318. <https://doi.org/10.1016/J.IJHYDENE.2019.11.092>.
- [12] T. Stehly, P. Duffy, D. Mulas Hernando, 2022 Cost of Wind Energy Review, (2023) 627281636.
- [13] IRNEA, IRENA (2022), Renewable Power Generation Costs in 2021, International Renewable Energy Agency, Abu Dhabi. ISBN 978-92-9260-452-3, Int. Renew. Energy Agency. (2022) 160. [https://www.irena.org/-/media/Files/IRENA/Agency/Publication/2018/Jan/IRENA\\_2017\\_Power\\_Costs\\_2018.pdf](https://www.irena.org/-/media/Files/IRENA/Agency/Publication/2018/Jan/IRENA_2017_Power_Costs_2018.pdf) (accessed March 30, 2024).
- [14] A. Smallbone, V. Jülch, R. Wardle, A.P. Roskilly, Levelised Cost of Storage for Pumped Heat Energy Storage in comparison with other energy storage technologies, *Energy Convers. Manag.* 152 (2017) 221–228. <https://doi.org/10.1016/J.ENCONMAN.2017.09.047>.